Supporting Information for

Paleoclimate pattern effects help constrain climate sensitivity and 21st-century warming

Vincent T. Cooper, Kyle C. Armour, Gregory J. Hakim, Jessica E. Tierney, Natalie J. Burls, Cristian Proistosescu, Timothy Andrews, Wenhao Dong, Michelle T. Dvorak, Ran Feng, Matthew B. Osman, Yue Dong

Vincent T. Cooper.
E-mail: vcooper@mit.edu

This PDF file includes:

Figs. S1 to S11
Tables S1 to S4
SI References

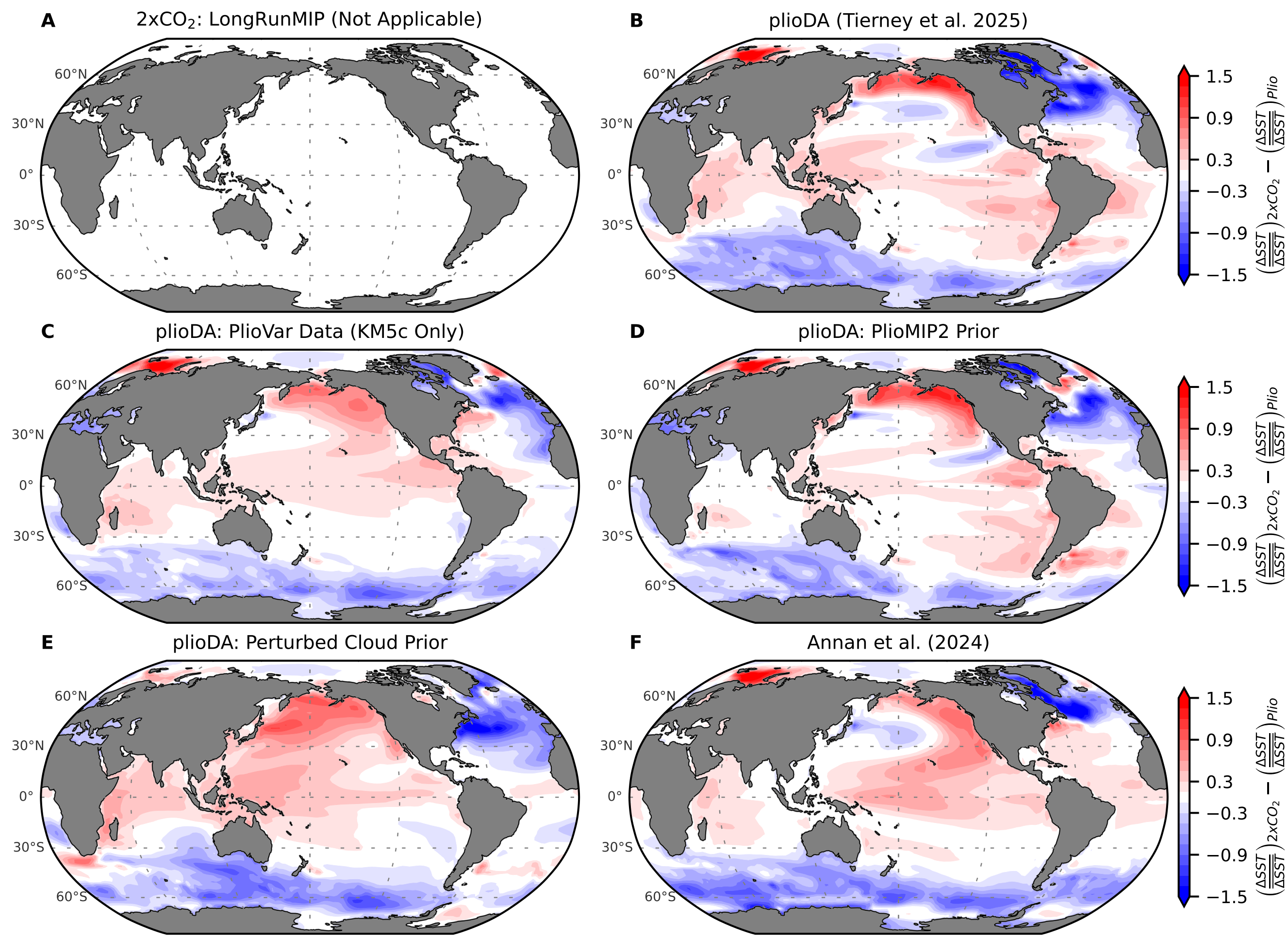

Fig. S1. Differences between the 2xCO$_2$ pattern of sea-surface temperature (SST) anomalies and Pliocene patterns of SST anomalies. Panels correspond to Figure 1 of Main Text; note that panel **A** is intentionally blank. Before taking the differences, each pattern's local anomalies are divided by its global-mean SST anomaly to emphasize the spatial patterns. Red regions indicate stronger relative amplification of warming in the LongRunMIP 2xCO$_2$ pattern (1), while blue regions indicate stronger relative amplification of Pliocene warming. See Figure S10 for zonal-mean SST anomalies and pattern differences.

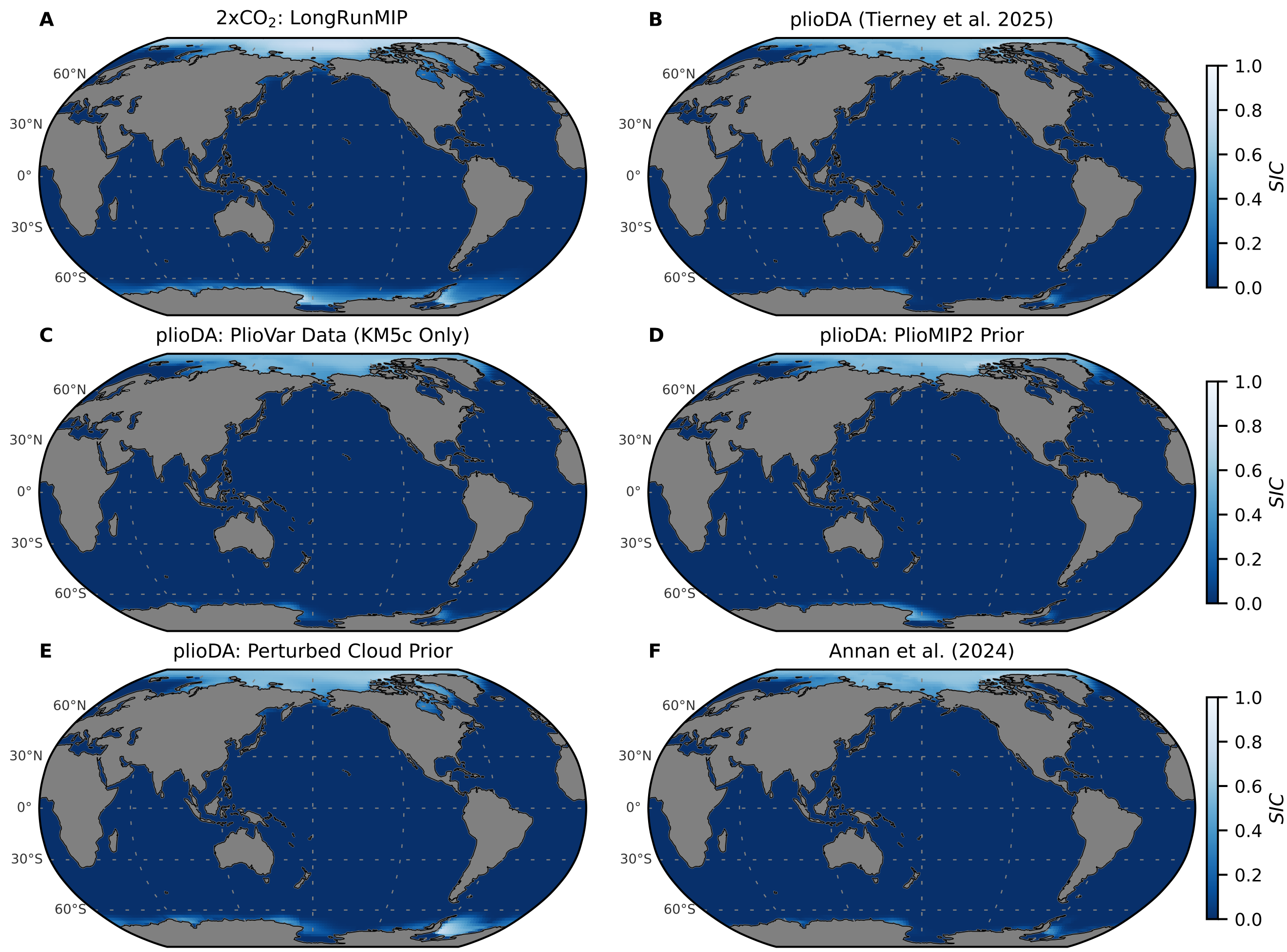

Fig. S2. Sea-ice concentration (SIC): LongRunMIP 2xCO_2 and Pliocene reconstructions. Panels correspond to Figure 1 of Main Text and show annual means. Note that plioDA sea ice is used for the Annan et al. (2024) reconstruction.

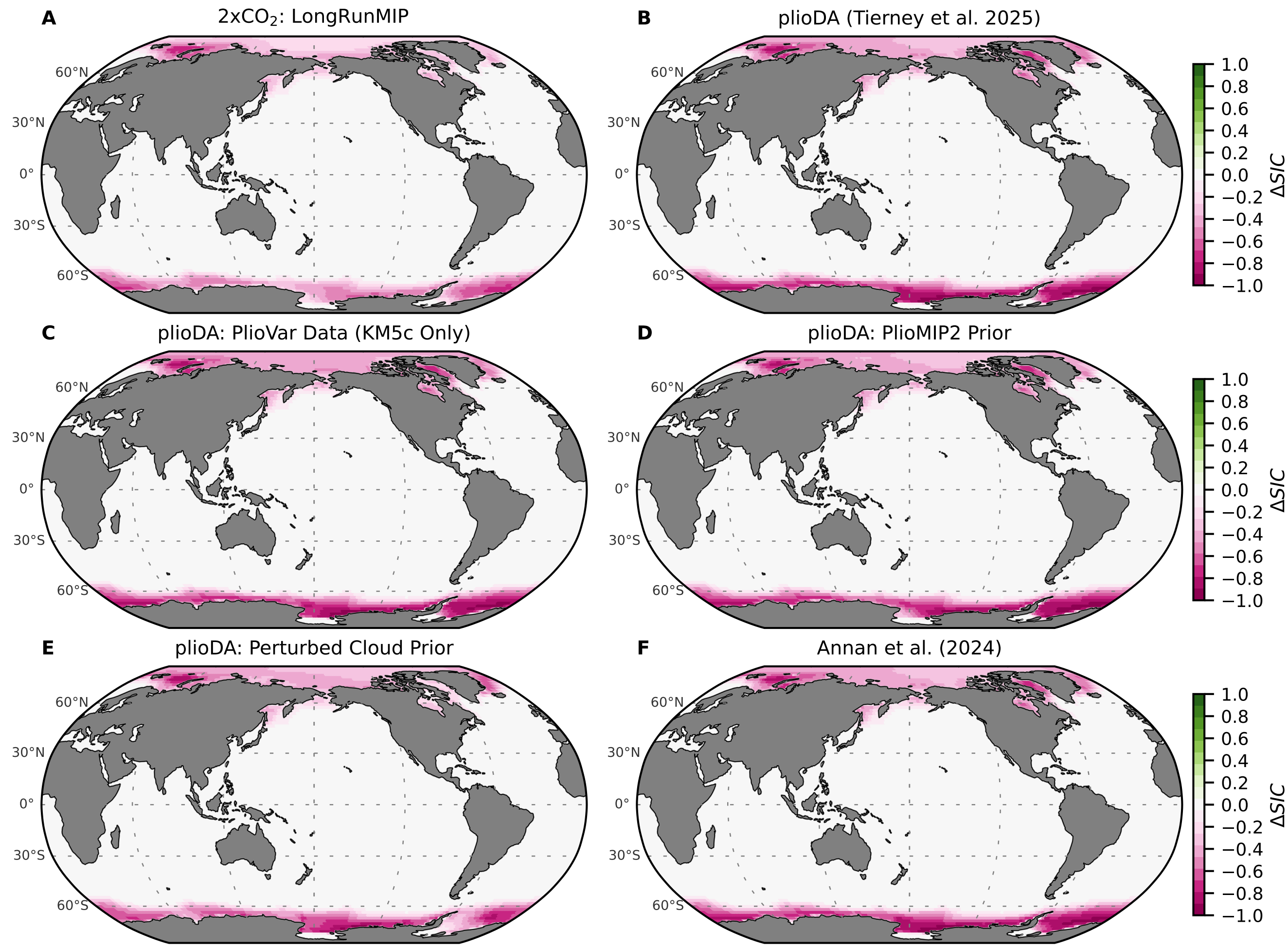

Fig. S3. Sea-ice concentration (SIC) anomalies: LongRunMIP 2xCO_2 and Pliocene reconstructions relative to preindustrial baseline. Panels correspond to Figure 1 of Main Text and show annual-mean differences relative to the preindustrial (Late Holocene) baseline (2). Note that plioDA sea ice is used for the Annan et al. (2024) reconstruction.

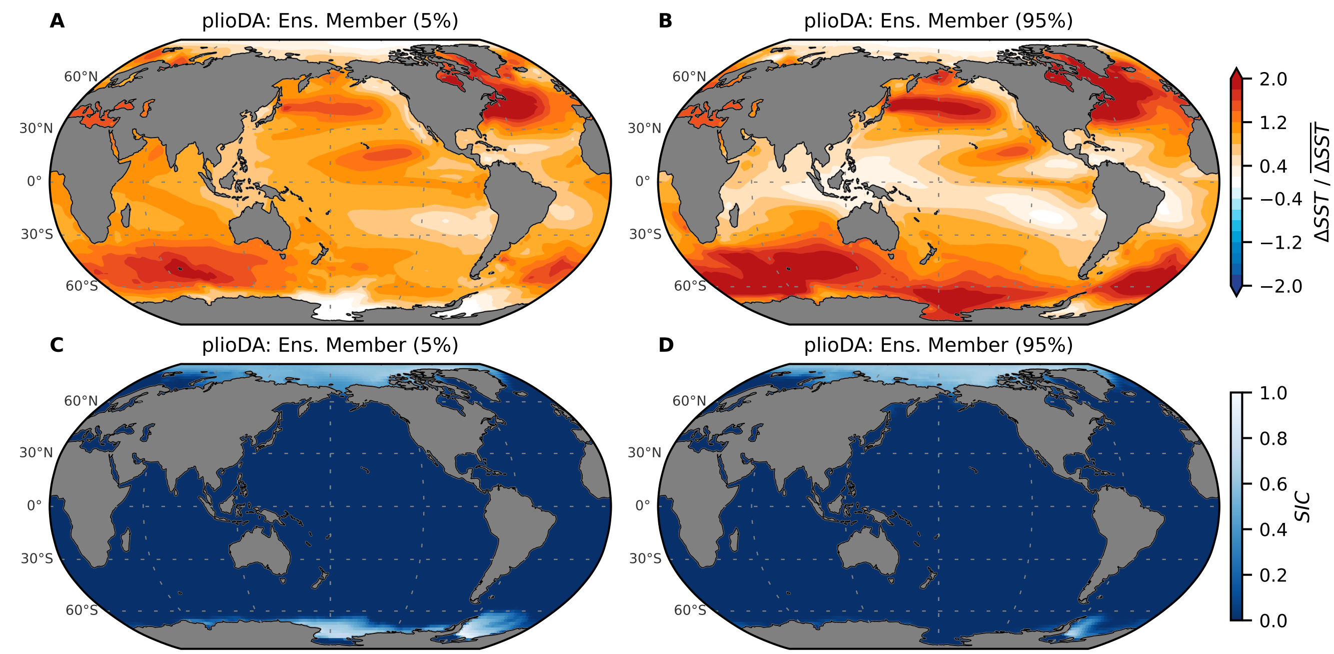

Fig. S4. 5th and 95th percentile ensemble members from plioDA reconstruction (3). **(A–B)** Sea-surface temperature (SST) anomalies and **(C–D)** sea-ice concentration (SIC) for ensemble members with the 5th percentile net feedback (more negative, stable climate) and 95th percentile net feedback (more positive, less stable climate). Ensemble members are ranked using CAM4 Green's functions (4) (Methods).

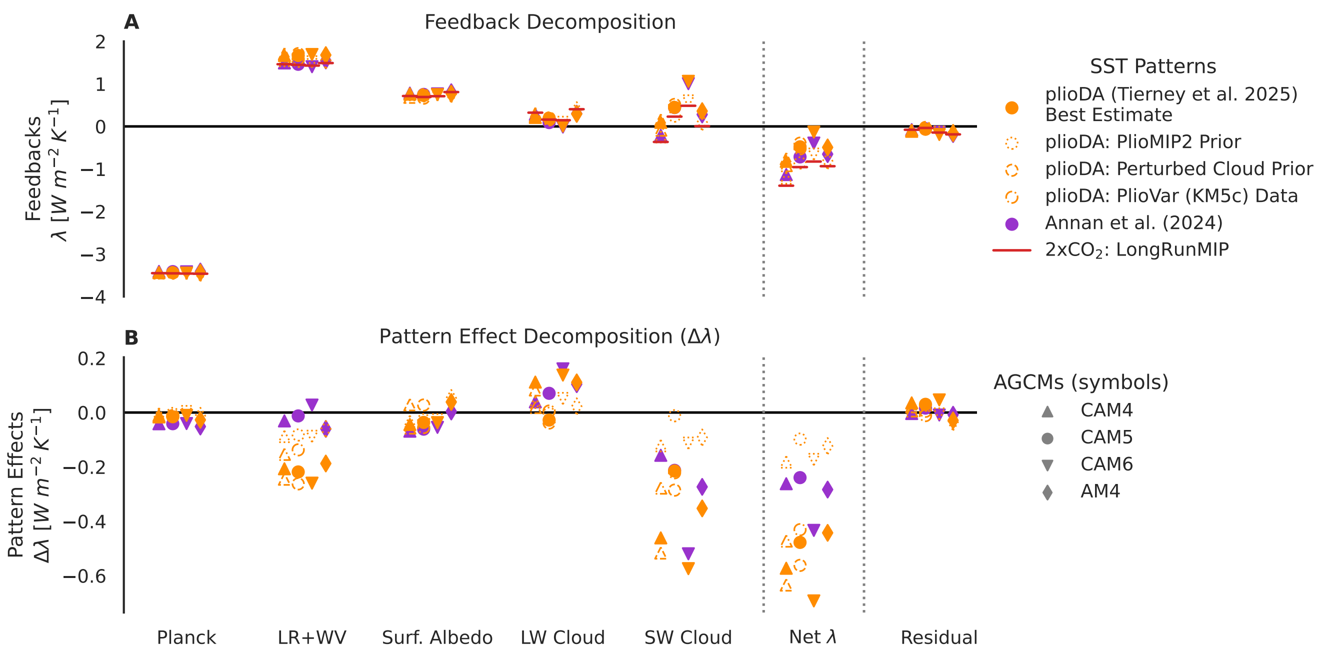

Fig. S5. Kernel decomposition of radiative feedbacks (λ)**.** Note that each legend applies to both panels: different sea-surface temperature and sea ice patterns are distinguished by colors/borders, while the different atmospheric general circulation models (AGCMs) are distinguished by symbol shapes. **(A)** Decomposition of feedbacks using radiative kernels (5) from CAM5 (6). **(B)** Pattern effects $(\Delta\lambda = \lambda_{\mathrm{2xCO_2}} - \lambda_{\mathrm{Plio}})$ for each component feedback in panel **A**. Planck represents the additional longwave emission to space from a vertically uniform change in atmospheric and surface temperatures (e.g., 5, 7–9), LR+WV represents the lapse rate and water vapor feedbacks, and LW and SW refer to longwave and shortwave radiation. Note that all kernel results exclude HadGEM3 due to limited availability of model output.

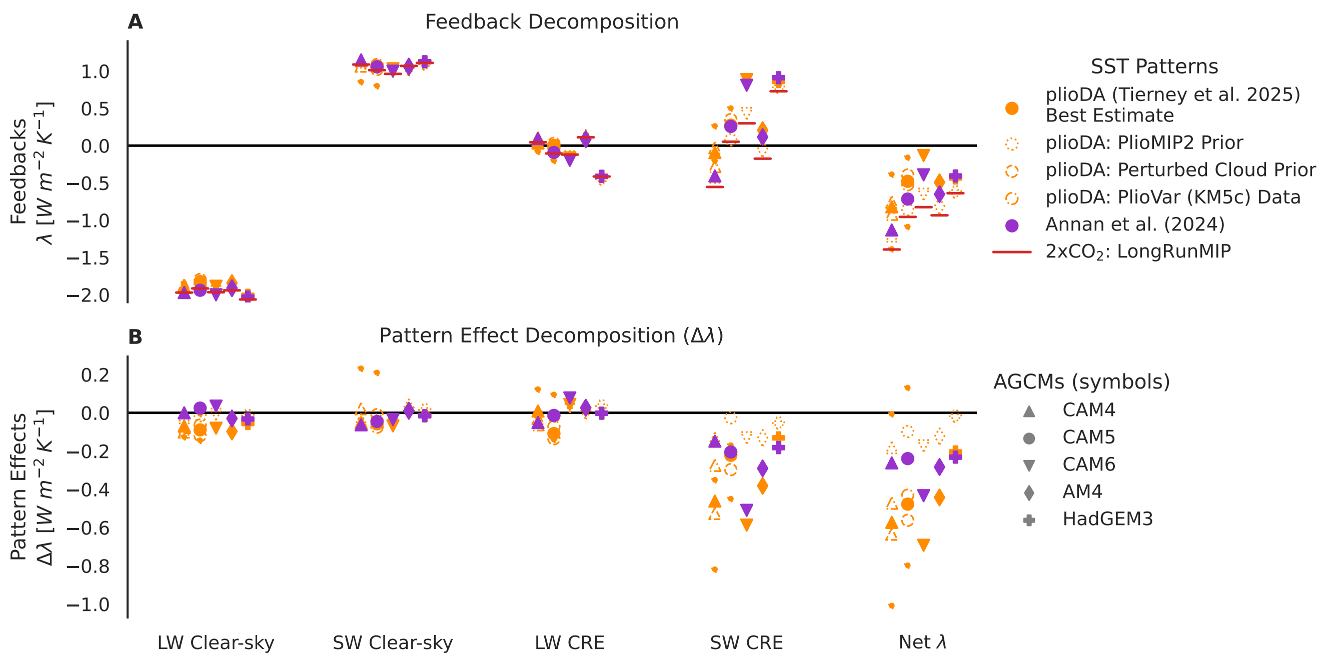

Fig. S6. Decomposition of radiative feedbacks (λ) from direct model outputs for clear-sky radiation and cloud radiative effects (CRE). Note that each legend applies to both panels: different sea-surface temperature and sea ice patterns are distinguished by colors/borders, while the different atmospheric general circulation models (AGCMs) are distinguished by symbol shapes. Results are separated into longwave (LW) and shortwave (SW) radiation components. **(A)** Decomposition of feedbacks, and **(B)** decomposition of pattern effects $(\Delta\lambda = \lambda_{2\mathrm{xCO}_2} - \lambda_{\mathrm{Plio}})$. Small orange dots show the 5th and 95th percentile members of the plioDA ensemble (Methods).

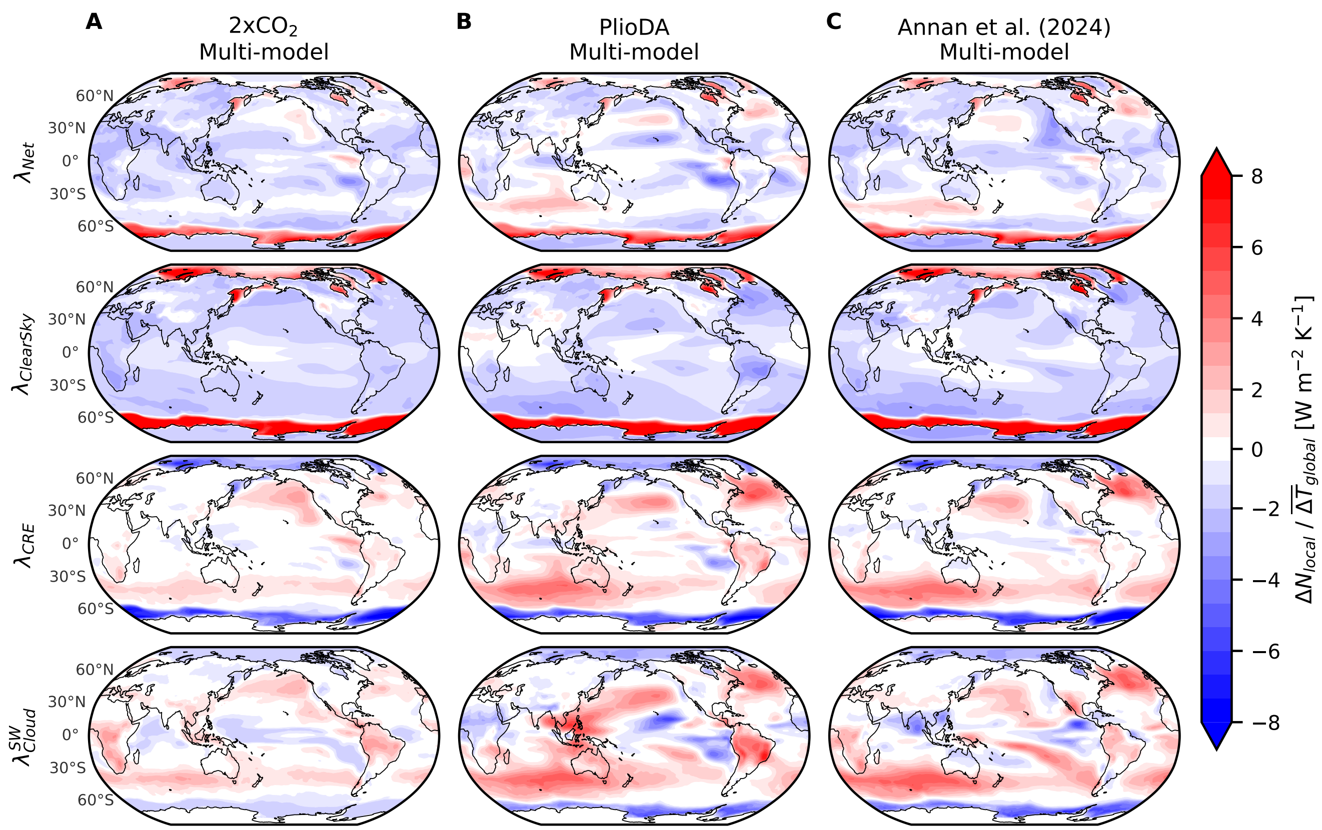

Fig. S7. Spatial pattern of local radiative feedbacks (λ)**.** Local feedbacks are calculated as $\Delta N/\overline{\Delta T}$, where ΔN is the local anomaly in top-of-atmosphere radiation, and $\overline{\Delta T}$ is the global-mean anomaly in near-surface air temperature. Multi-model mean, including CAM4, CAM5, CAM6, GFDL-AM4, and HadGEM3 from **(A)** LongRunMIP 2xCO_2 (1), **(B)** plioDA (3), and **(C)** Annan et al. (10). CRE refers to cloud radiative effects, while SW cloud refers to shortwave cloud feedbacks estimated with radiative kernels (5, 6). Note that kernel results (for SW cloud in bottom row) exclude HadGEM3 due to limited availability of model output.

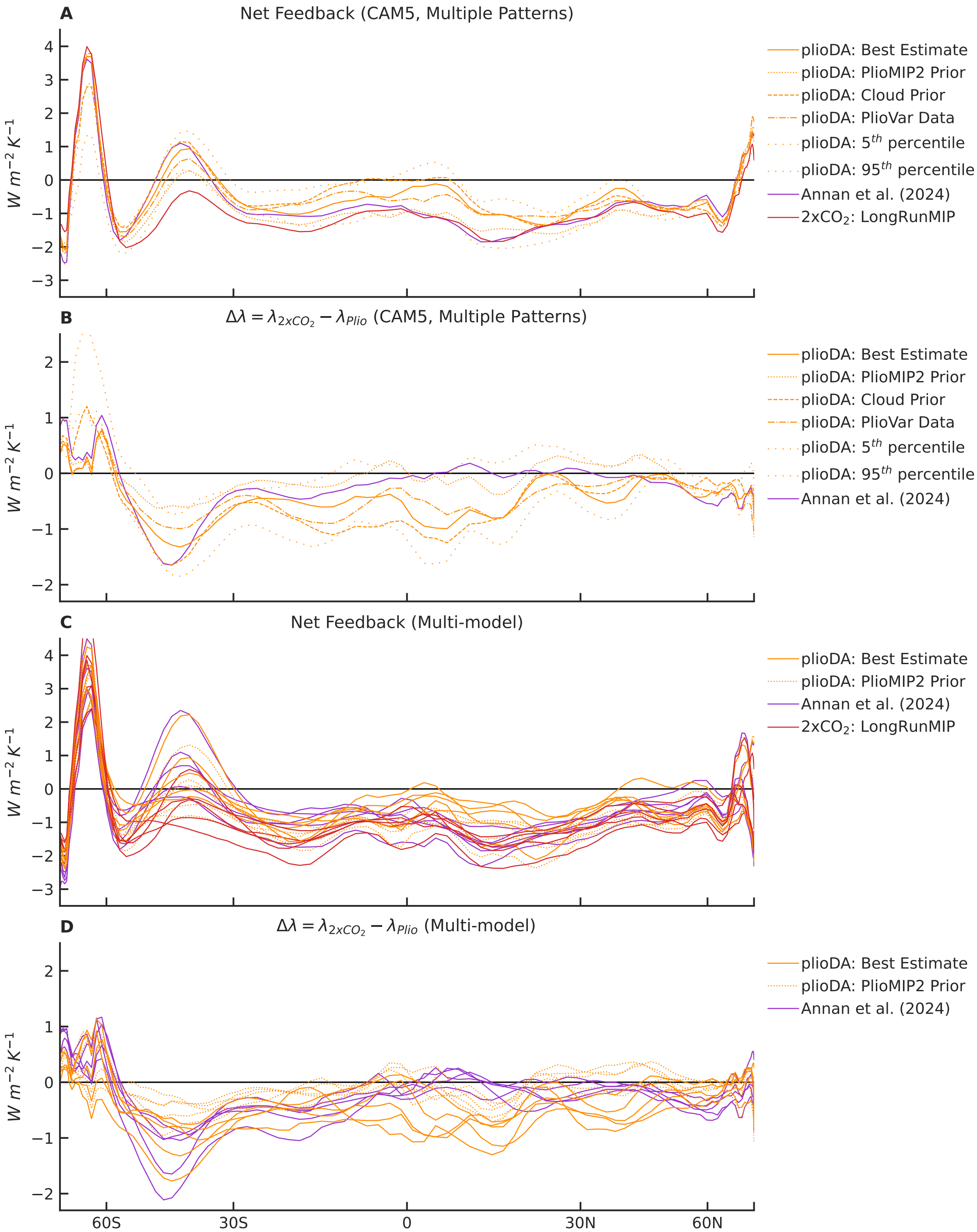

Fig. S8. Zonal mean of local net feedbacks (λ) and pattern effects, $\Delta\lambda = \lambda_{2\mathrm{xCO}_2} - \lambda_{\mathrm{Plio}}$. Local feedbacks are calculated as $\Delta N/\overline{\Delta T}$, where ΔN is the local anomaly in top-of-atmosphere radiation, and $\overline{\Delta T}$ is the global-mean anomaly in near-surface air temperature. **(A)** Feedbacks in CAM5 using various patterns of sea-surface temperature (SST) and sea ice, and **(B)** Pattern effects, $\Delta\lambda = \lambda_{2\mathrm{xCO}_2} - \lambda_{\mathrm{Plio}}$, in CAM5 corresponding to panel **A**. **(C–D)** Repeat of panels **A–B** showing the subset of SST and sea ice patterns used in all five models (CAM4, CAM5, CAM6, GFDL-AM4, and HadGEM3); each line listed on the legends for panels **C–D** is shown multiple times in the figure to represent each of the five models.

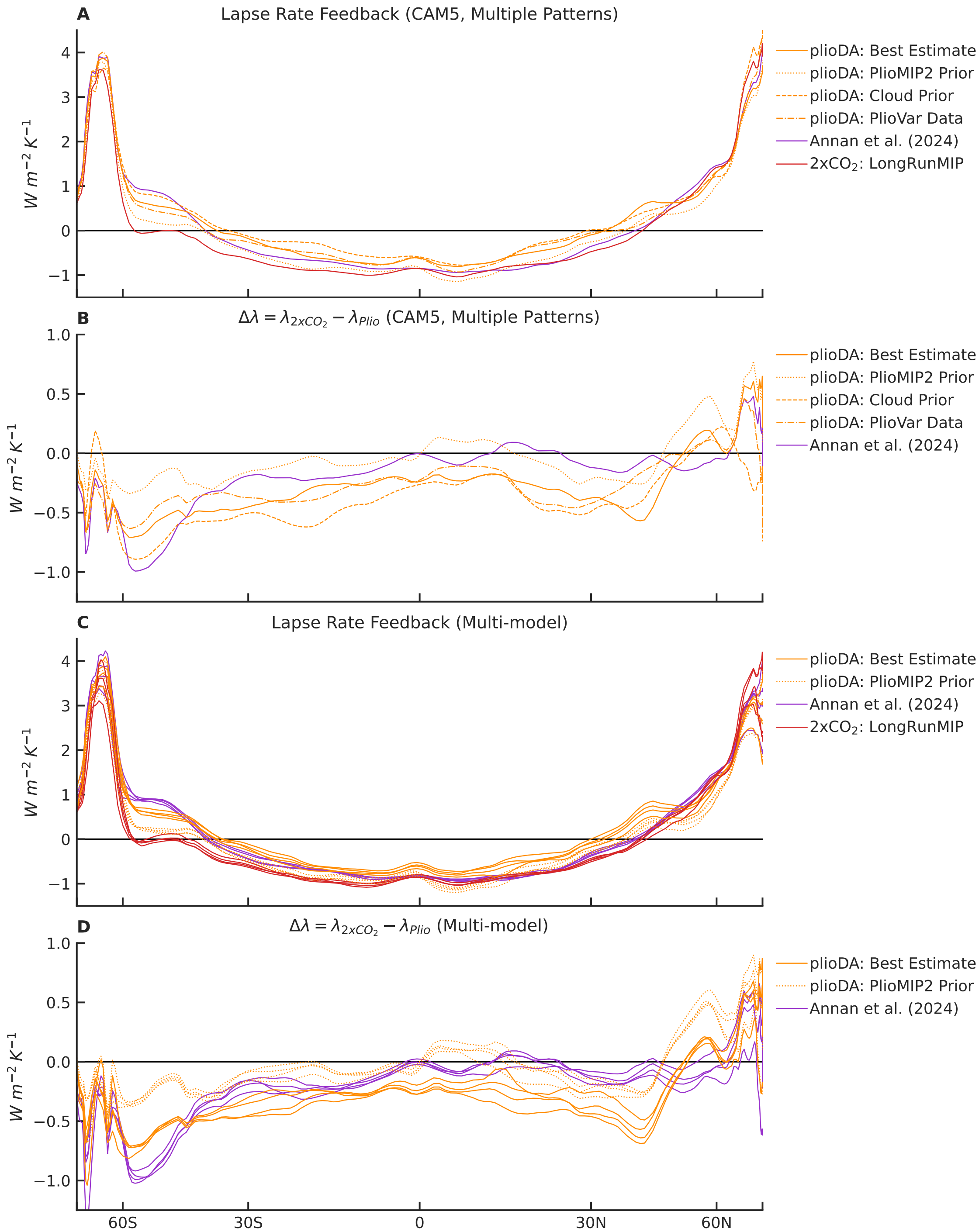

Fig. S9. Zonal mean of local lapse rate feedbacks (λ) and pattern effects, $\Delta\lambda = \lambda_{2\mathrm{xCO_2}} - \lambda_{\mathrm{Plio}}$. Local feedbacks are calculated as $\Delta N/\overline{\Delta T}$, where ΔN is the local anomaly in top-of-atmosphere radiation, and $\overline{\Delta T}$ is the global-mean anomaly in near-surface air temperature. **(A)** Feedbacks in CAM5 using various patterns of sea-surface temperature (SST) and sea ice, and **(B)** Pattern effects, $\Delta\lambda = \lambda_{2\mathrm{xCO_2}} - \lambda_{\mathrm{Plio}}$, in CAM5 corresponding to panel **A**. **(C–D)** Repeat of panels **A–B** showing the subset of SST and sea ice patterns used in all five models (CAM4, CAM5, CAM6, GFDL-AM4, and HadGEM3); each line listed on the legends for panels **C–D** is shown multiple times in the figure to represent each of the five models. Note that this figure shows kernel results for a subset of patterns and only four models (excludes HadGEM3) due to limited availability of model output.

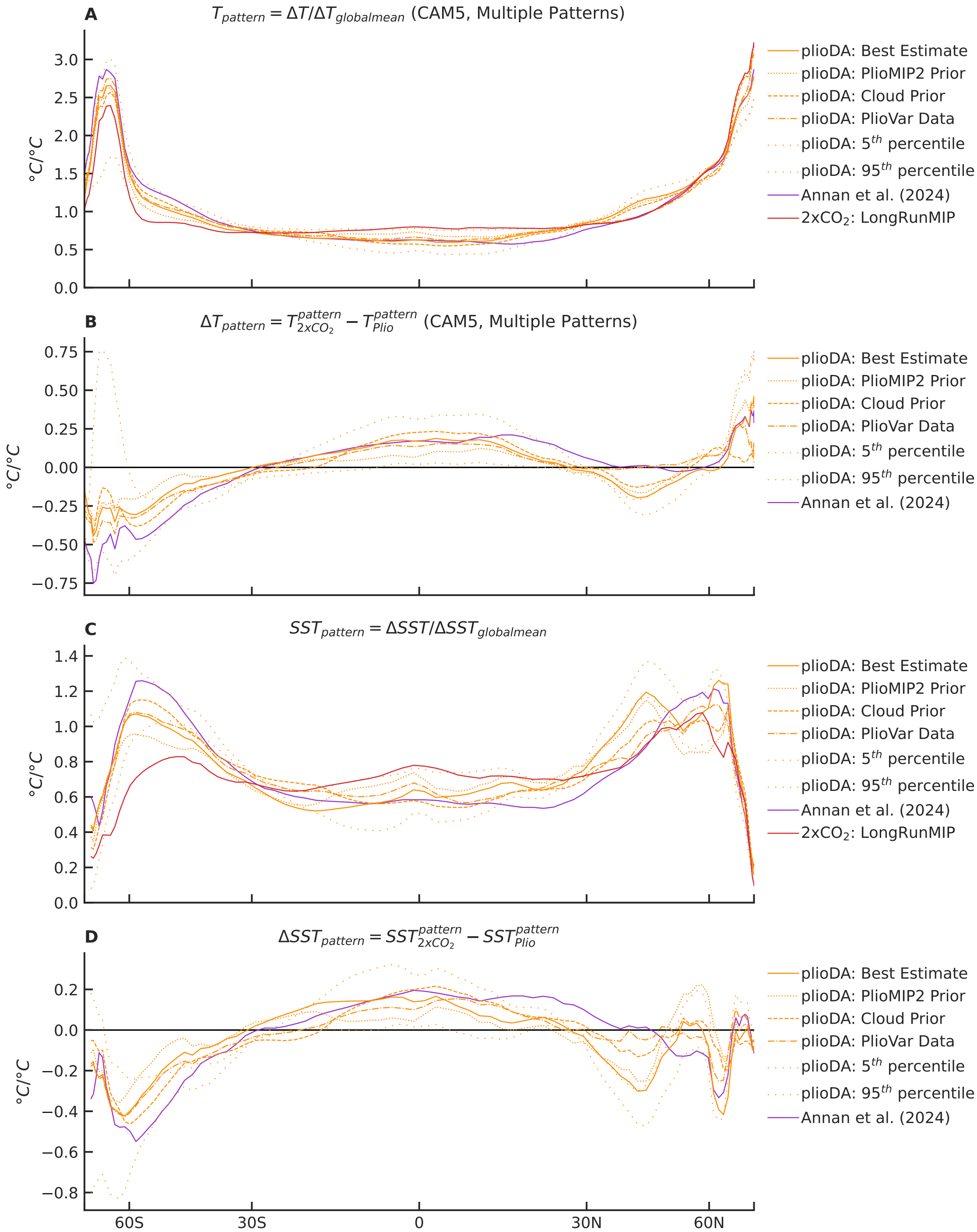

Fig. S10. Zonal-mean patterns of temperature anomalies. (A) Normalized near-surface air T from various patterns and **(B)** differences versus LongRunMIP 2xCO$_2$ pattern. **(C–D)** Repeats panels **A** and **B** for SST. Note that **A–B** show AGCM output from CAM5, whereas **C–D** show input boundary conditions for all AGCMs.

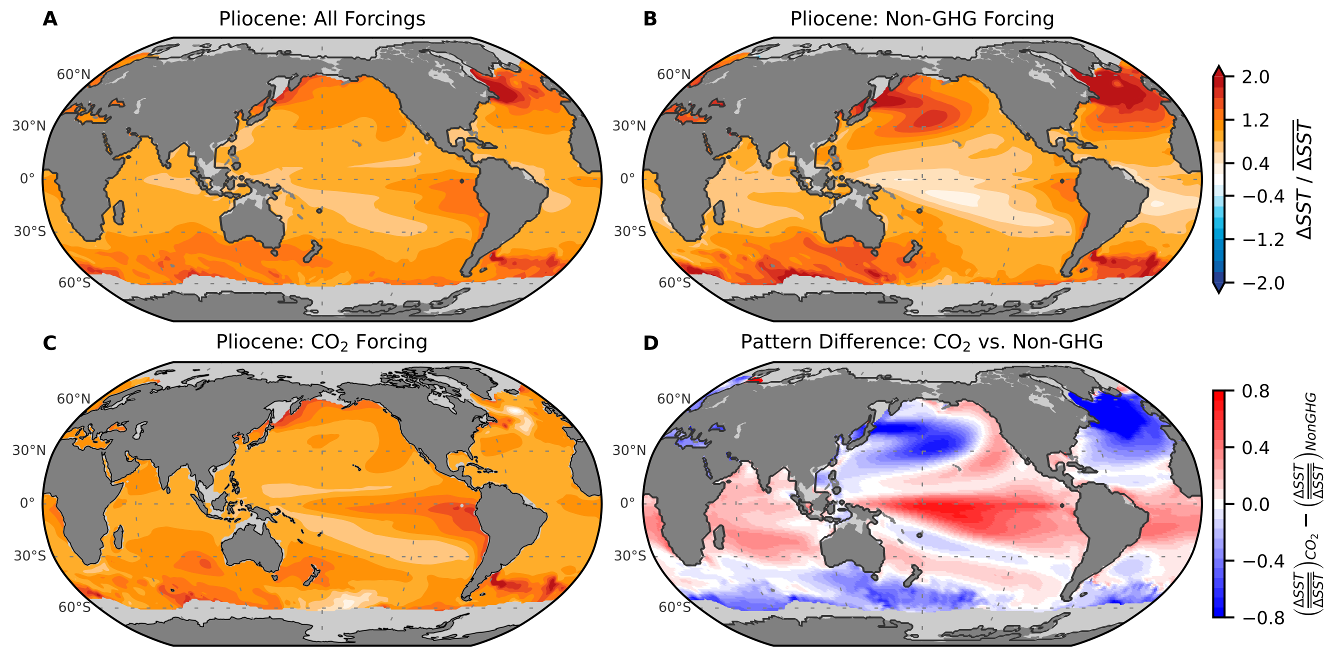

Fig. S11. Sea-surface temperature (SST) response to Pliocene forcings in CESM2.1 from ref. (11). (A–C) Patterns of SST anomalies (normalized by global-mean anomalies) relative to preindustrial control from **(A)** all Pliocene forcings, **(B)** Non-GHG forcings including ice sheets, vegetation, topography, and bathymetry, and **(C)** CO_2 concentration of 400 ppm, which accounts for both CO_2 and methane forcing. **(D)** Difference between SST response to CO_2 versus non-GHG forcing, represented as panel **C** minus panel **B**; red regions indicate stronger relative amplification of warming from CO_2, while blue regions indicate stronger relative amplification from non-GHG forcings. In all panels, regions of preindustrial sea ice are masked in light gray. The CESM2 simulations follow the PlioMIP2 protocol (12, 13).

Table S1. All units are $\mathrm{W\,m^{-2}\,K^{-1}}$. Pliocene pattern effects, $\Delta\lambda = \lambda_{2xCO_2} - \lambda_{Plio}$, from three patterns of reconstructed Pliocene SST and sea ice in various AGCMs (CAM4 coupled to CLM4.5, CAM5.3 coupled to CLM5.0, CAM6.0 coupled to CLM5.0, GFDL-AM4.0, and HadGEM3-GC3.1-LL). Alternate values for Pliocene pattern effects, $\Delta\lambda^{Alt}_{150yr} = \lambda^{CO_2}_{150yr} - \lambda_{Plio}$, are shown using 150-yr regression of abrupt-4xCO_2 simulations (abrupt-2xCO_2 is used for CESM2.1-CAM6.0 to avoid issues with the ice nucleation scheme and cloud microphysics timestep (14, 15) that impact the feedback diagnosed from the 4xCO_2 simulation) from coupled models corresponding to each AGCM (16).

Model	Pattern	$\Delta\lambda$	λ_{Plio}	λ_{2xCO_2}	$\Delta\lambda^{Alt}_{150yr}$	$\lambda^{CO_2}_{150yr}$
CAM4	plioDA	-0.57	-0.82	-1.39	-0.41	-1.23
CAM4	plioDA: PlioMIP2 Prior	-0.18	-1.21	-1.39	-0.02	-1.23
CAM4	Annan24	-0.26	-1.13	-1.39	-0.10	-1.23
CAM5	plioDA	-0.48	-0.48	-0.96	-0.67	-1.15
CAM5	plioDA: PlioMIP2 Prior	-0.10	-0.86	-0.96	-0.29	-1.15
CAM5	Annan24	-0.24	-0.72	-0.96	-0.43	-1.15
CAM6	plioDA	-0.69	-0.13	-0.83	-1.08	-1.21
CAM6	plioDA: PlioMIP2 Prior	-0.17	-0.65	-0.83	-0.56	-1.21
CAM6	Annan24	-0.43	-0.39	-0.83	-0.82	-1.21
GFDL-AM4	plioDA	-0.44	-0.49	-0.93	-0.37	-0.86
GFDL-AM4	plioDA: PlioMIP2 Prior	-0.12	-0.81	-0.93	-0.05	-0.86
GFDL-AM4	Annan24	-0.28	-0.65	-0.93	-0.21	-0.86
HadGEM3	plioDA	-0.20	-0.44	-0.64	-0.19	-0.63
HadGEM3	plioDA: PlioMIP2 Prior	-0.02	-0.62	-0.64	-0.01	-0.63
HadGEM3	Annan24	-0.24	-0.41	-0.64	-0.22	-0.63
CAM4	mean	-0.34	-1.05	-1.39	-0.18	-1.23
CAM5	mean	-0.27	-0.68	-0.96	-0.47	-1.15
CAM6	mean	-0.43	-0.39	-0.83	-0.82	-1.21
GFDL-AM4	mean	-0.28	-0.65	-0.93	-0.21	-0.86
HadGEM3	mean	-0.15	-0.49	-0.64	-0.14	-0.63
mean	Annan24	-0.29	-0.66	-0.95	-0.36	-1.02
mean	plioDA	-0.48	-0.47	-0.95	-0.54	-1.02
mean	plioDA: PlioMIP2 Prior	-0.12	-0.83	-0.95	-0.18	-1.02
mean	**mean**	-0.30	-0.65	-0.95	-0.36	-1.02
1σ	1σ	0.19	0.29		0.31	

Table S2. Pliocene pattern effects, $\Delta\lambda = \lambda_{2xCO_2} - \lambda_{Plio}$, from various patterns of reconstructed Pliocene SST and sea ice in CAM4 and CAM5. Global-mean anomalies for SST, near-surface air temperature (T), and top-of-atmosphere radiative imbalance (N) are shown for reference. Alternate values for Pliocene pattern effects, $\Delta\lambda^{Alt}_{150yr} = \lambda^{CO_2}_{150yr} - \lambda_{Plio}$, are shown using 150-yr regression feedbacks (Table S1).

Units		$Wm^{-2}K^{-1}$	$Wm^{-2}K^{-1}$	K	K	Wm^{-2}	$Wm^{-2}K^{-1}$
Model	Pattern	$\Delta\lambda$	λ	ΔSST	ΔT	ΔN	$\Delta\lambda^{Alt}_{150yr}$
CAM4	plioDA	-0.57	-0.82	3.00	3.90	-3.20	-0.41
CAM4	plioDA: PlioVar Data	-0.47	-0.92	2.89	3.78	-3.48	-0.31
CAM4	plioDA: PlioMIP2 Prior	-0.18	-1.21	2.94	3.86	-4.67	-0.02
CAM4	plioDA: Cloud Prior	-0.63	-0.76	2.83	3.68	-2.79	-0.47
CAM4	plioDA: 5%	-0.01	-1.39	3.96	4.88	-6.77	0.16
CAM4	plioDA: 95%	-1.01	-0.38	3.29	4.02	-1.55	-0.85
CAM4	Annan24	-0.26	-1.13	2.82	3.72	-4.21	-0.10
CAM4	**mean**	-0.45	-0.94	3.10	3.98	-3.81	-0.29
CAM4	$\mathbf{1\sigma}$	0.33	0.33	0.41	0.41	1.65	0.33
CAM4	*2xCO2: LongRunMIP*		-1.39	2.35	3.16	-4.40	

Model	Pattern	$\Delta\lambda$	λ	ΔSST	ΔT	ΔN	$\Delta\lambda^{Alt}_{150yr}$
CAM5	plioDA	-0.48	-0.48	3.00	3.98	-1.90	-0.67
CAM5	plioDA: PlioVar Data	-0.43	-0.53	2.89	3.85	-2.02	-0.62
CAM5	plioDA: PlioMIP2 Prior	-0.10	-0.86	2.94	3.96	-3.40	-0.29
CAM5	plioDA: Cloud Prior	-0.56	-0.39	2.83	3.75	-1.48	-0.76
CAM5	plioDA: 5%	0.13	-1.09	3.96	4.99	-5.42	-0.06
CAM5	plioDA: 95%	-0.80	-0.16	3.29	4.10	-0.65	-0.99
CAM5	Annan24	-0.24	-0.72	2.82	3.78	-2.71	-0.43
CAM5	**mean**	-0.35	-0.60	3.10	4.06	-2.51	-0.55
CAM5	$\mathbf{1\sigma}$	0.31	0.31	0.41	0.43	1.55	0.31
CAM5	*2xCO2: LongRunMIP*		-0.96	2.35	3.21	-3.07	

Table S3. Posterior distributions of climate sensitivity (S). "Combined Evidence" assumes the Baseline Prior, $\lambda \sim \mathrm{Unif}(-10, 10)\ \mathrm{W\,m^{-2}\,K^{-1}}$, and includes Process Understanding, Historical Evidence, and Paleoclimate Evidence from the Last Glacial Maximum (LGM) and Pliocene. The Robust Range also combines lines of evidence but assumes a Uniform S Prior, $S \sim \mathrm{Unif}(0, 20)\ K$ (17). "Pliocene Only" considers only Pliocene evidence and assumes the Uniform S Prior. All uncertainties shown are 1σ values. Table structure is comparable to Table 10 of Sherwood, Webb et al. (2020).

Combined Evidence (Baseline Prior)	5th	17th	50th	83rd	95th	Mean	ΔT_{Plio}	ΔF^{Plio}_{NonGHG}	ΔT_{LGM}
SW20: Original	2.3	2.6	3.1	3.9	4.7	3.2	3.0 $\pm$ 1.0	f_{ESS}	-5 $\pm$ 1
+ Update ΔT_{LGM}	2.3	2.7	3.2	4.1	5.0	3.4	3.0 $\pm$ 1.0	f_{ESS}	-6 $\pm$ 1
+ Update ΔT_{Plio}	2.6	2.9	3.6	4.6	5.6	3.8	4.1 $\pm$ 0.6	f_{ESS}	-6 $\pm$ 1
+ Update ΔF^{Plio}_{NonGHG}	2.5	2.8	3.4	4.3	5.2	3.6	4.1 $\pm$ 0.6	1.7 $\pm$ 1.0	-6 $\pm$ 1
Include only LGM $\Delta\lambda$	2.3	2.6	3.0	3.7	4.4	3.2	4.1 $\pm$ 0.6	1.7 $\pm$ 1.0	-6 $\pm$ 1
Include only Pliocene $\Delta\lambda$	2.3	2.6	3.1	3.9	4.7	3.3	4.1 $\pm$ 0.6	1.7 $\pm$ 1.0	-6 $\pm$ 1
Full Update incl. Paleo $\Delta\lambda$	**2.1**	**2.4**	**2.8**	**3.4**	**4.0**	**2.9**	4.1 $\pm$ 0.6	1.7 $\pm$ 1.0	-6 $\pm$ 1
Alt. Update incl. Paleo $\Delta\lambda^{\mathrm{Alt}}_{150\mathrm{yr}}$	2.1	2.4	2.8	3.5	4.1	3.0	4.1 $\pm$ 0.6	1.7 $\pm$ 1.0	-6 $\pm$ 1

Combined, Robust Range (Unif. S Prior)	5th	17th	50th	83rd	95th	Mean	ΔT_{Plio}	ΔF^{Plio}_{NonGHG}	ΔT_{LGM}
SW20: Original Robust Range (Unif. S)	2.4	2.8	3.5	4.5	5.7	3.7	3.0 $\pm$ 1.0	f_{ESS}	-5 $\pm$ 1
+ Update $\Delta T,\ \Delta F^{Plio}_{NonGHG}$ (Unif. S)	2.6	3.0	3.8	4.9	6.2	4.0	4.1 $\pm$ 0.6	1.7 $\pm$ 1.0	-6 $\pm$ 1
Full Update incl. Paleo $\Delta\lambda$ (Unif. S)	2.3	2.6	3.1	3.8	4.6	3.2	4.1 $\pm$ 0.6	1.7 $\pm$ 1.0	-6 $\pm$ 1
Alt. Update incl. Paleo $\Delta\lambda^{\mathrm{Alt}}_{150\mathrm{yr}}$ (Unif. S)	2.3	2.6	3.1	3.9	4.8	3.3	4.1 $\pm$ 0.6	1.7 $\pm$ 1.0	-6 $\pm$ 1

Pliocene Only (Unif. S Prior)	5th	17th	50th	83rd	95th	Mean	ΔT_{Plio}	ΔF^{Plio}_{NonGHG}
SW20: Original	1.6	2.4	4.0	6.8	10.1	4.7	3.0 $\pm$ 1.0	f_{ESS}
+ Update ΔT_{Plio}	2.9	3.8	5.6	8.6	12.3	6.3	3.0 $\pm$ 1.0	f_{ESS}
+ Update ΔF^{Plio}_{NonGHG}	2.5	3.2	4.7	7.4	11.2	5.4	4.1 $\pm$ 0.6	1.7 $\pm$ 1.0
Include Pliocene $\Delta\lambda$	1.9	2.4	3.8	7.2	12.9	5.0	4.1 $\pm$ 0.6	1.7 $\pm$ 1.0
Alt. Pliocene $\Delta\lambda^{\mathrm{Alt}}_{150\mathrm{yr}}$	1.8	2.4	3.8	8.3	14.8	5.3	4.1 $\pm$ 0.6	1.7 $\pm$ 1.0

Units in $^\circ$C; ΔF units in $\mathrm{W\,m^{-2}}$.

Table S4. Paired estimates of Pliocene and LGM pattern effects, which use similar methods for data assimilation and the same AGCMs. The pairs are used to estimate the Pearson correlation and covariance between estimates of Pliocene and LGM pattern effects (18). For the standard $\Delta\lambda, r = 0.56$ and $\mathrm{cov} = 0.0123$ $[\mathrm{W\ m^{-2}\ K^{-1}}]^2$. For $\Delta\lambda^{\mathrm{Alt}}_{\mathrm{150yr}}$, $r = 0.87$ and $\mathrm{cov} = 0.0562$ $[\mathrm{W\ m^{-2}\ K^{-1}}]^2$. Table units are $\mathrm{W\ m^{-2}\ K^{-1}}$. LGM results use updated CESM2.1 $\lambda^{\mathrm{Alt}}_{\mathrm{150yr}}$ in Table S1.

AGCM	Plio Pattern	LGM Pattern	$\Delta\lambda_{\mathrm{Plio}}$	$\Delta\lambda_{\mathrm{LGM}}$	$\Delta\lambda^{\mathrm{Alt150}}_{\mathrm{Plio}}$	$\Delta\lambda^{\mathrm{Alt150}}_{\mathrm{LGM}}$
CAM4	plioDA	LGMR	-0.57	-0.45	-0.41	-0.21
CAM5	plioDA	LGMR	-0.48	-0.31	-0.67	-0.41
CAM6	plioDA	LGMR	-0.69	-0.63	-1.08	-1.02
AM4	plioDA	LGMR	-0.44	-0.33	-0.37	-0.27
HadGEM3	plioDA	LGMR	-0.20	-0.27	-0.19	-0.29
CAM4	Annan	Annan	-0.57	-0.29	-0.10	-0.06
CAM5	Annan	Annan	-0.48	-0.09	-0.43	-0.18
CAM4	plioDA: Cloud Prior	LGMR	-0.63	-0.45	-0.47	-0.21
CAM5	plioDA: Cloud Prior	LGMR	-0.56	-0.31	-0.76	-0.41
CAM4	plioDA: Cloud Prior	lgmDA	-0.63	-0.69	-0.47	-0.45
CAM5	plioDA: Cloud Prior	lgmDA	-0.56	-0.51	-0.76	-0.61
CAM4	plioDA	lgmDA	-0.57	-0.69	-0.41	-0.45
CAM5	plioDA	lgmDA	-0.48	-0.51	-0.67	-0.61

References

1. M Rugenstein, et al., LongRunMIP: Motivation and Design for a Large Collection of Millennial-Length AOGCM Simulations. *Bull. Am. Meteorol. Soc.* **100**, 2551–2570 (2019).
2. MB Osman, et al., Globally resolved surface temperatures since the Last Glacial Maximum. *Nature* **599**, 239–244 (2021).
3. JE Tierney, et al., Pliocene Warmth and Patterns of Climate Change Inferred From Paleoclimate Data Assimilation. *AGU Adv.* **6** (2025).
4. Y Dong, C Proistosescu, KC Armour, DS Battisti, Attributing Historical and Future Evolution of Radiative Feedbacks to Regional Warming Patterns using a Green's Function Approach: The Preeminence of the Western Pacific. *J. Clim.* **32**, 5471–5491 (2019).
5. BJ Soden, et al., Quantifying Climate Feedbacks Using Radiative Kernels. *J. Clim.* **21**, 3504–3520 (2008).
6. AG Pendergrass, A Conley, FM Vitt, Surface and top-of-atmosphere radiative feedback kernels for CESM-CAM5. *Earth Syst. Sci. Data* **10**, 317–324 (2018).
7. TW Cronin, I Dutta, How Well do We Understand the Planck Feedback? *J. Adv. Model. Earth Syst.* **15** (2023).
8. P Forster, et al., 2021: The Earth's energy budget, climate feedbacks, and climate sensitivity in *Climate Change 2021: The Physical Science Basis. Contribution of Working Group I to the Sixth Assessment Report of the Intergovernmental Panel on Climate Change*, eds. V Masson-Delmotte, et al. (Cambridge Univ. Press, Cambridge, UK and New York, NY), (2021).
9. MD Zelinka, et al., Causes of Higher Climate Sensitivity in CMIP6 Models. *Geophys. Res. Lett.* **47** (2020).
10. JD Annan, JC Hargreaves, T Mauritsen, E McClymont, SL Ho, Can we reliably reconstruct the mid-Pliocene Warm Period with sparse data and uncertain models? *Clim. Past* **20**, 1989–1999 (2024).
11. M Dvorak, et al., Mid-Pliocene Climate Forcing, Sea Surface Temperature Patterns, and Implications for Modern-Day Climate Sensitivity. *J. Clim.* **38**, 3037–3053 (2025).
12. AM Haywood, et al., The Pliocene Model Intercomparison Project Phase 2: large-scale climate features and climate sensitivity. *Clim. Past* **16**, 2095–2123 (2020).
13. R Feng, et al., Past terrestrial hydroclimate sensitivity controlled by Earth system feedbacks. *Nat. Commun.* **13**, 1306 (2022).
14. J Zhu, et al., LGM Paleoclimate Constraints Inform Cloud Parameterizations and Equilibrium Climate Sensitivity in CESM2. *J. Adv. Model. Earth Syst.* **14**, e2021MS002776 (2022).
15. N Burls, N Sagoo, Increasingly Sophisticated Climate Models Need the Out-Of-Sample Tests Paleoclimates Provide. *J. Adv. Model. Earth Syst.* **14** (2022).
16. T Andrews, et al., On the Effect of Historical SST Patterns on Radiative Feedback. *J. Geophys. Res. Atmospheres* **127** (2022).
17. SC Sherwood, et al., An Assessment of Earth's Climate Sensitivity Using Multiple Lines of Evidence. *Rev. Geophys.* **58** (2020).
18. VT Cooper, et al., Last Glacial Maximum pattern effects reduce climate sensitivity estimates. *Sci. Adv.* **10**, 9461 (2024).